Letters

3-D Embedded Receiving Coil Positioning Based on Decoupled Transformer for Wireless Sensor Power Supply System

Jing Li, Fuao Chen, Runze Zhu, Yang Chen, *Senior Member, IEEE*, and Ruikun Mai, *Senior Member, IEEE*

***Abstract*—Embedded sensors in structural health monitoring systems can be powered by wireless power transfer technology. However, misalignment between the transmitter and receiver is unavoidable, resulting in system efficiency and power decreases. To address this challenge, a 3-D positioning method for the embedded receiving coil based on a decoupled transformer is proposed. The decoupled transformer consists of two helical coils and one planar coil. These three coils are orthogonal to each other and decoupled magnetically. Coupling occurs only between the decoupled transformer and the receiving coil. This method requires neither auxiliary sources nor communication equipment, and it does not involve complex control. Experimental results show that when the transmission distance ranges from 50 to 80 mm, 93% of the positioning errors are within 10 mm in a 140 mm × 140 mm area. It is proved that the proposed method achieves a high accuracy.**

***Index Terms*—Coil positioning, decoupled transformer, embedded sensor, wireless power transfer (WPT).**

I. Introduction

EMBEDDED sensors can continuously collect vital data, such as stress, displacement, temperature, and so on, playing an important role in structural health monitoring systems. In recent years, wireless power transfer technology has attracted widespread attention due to its convenience and flexibility, offering an effective power supply solution for embedded sensors [1], [2].

In a wireless sensor power supply (WSPS) system, the receiving coil and sensors are embedded within the concrete, while the transmitting coil is typically carried by movable equipment, such as robots or drones. For example, Fig. 1 depicts a WSPS system where a drone carries the transmitting coil, generating an alternating magnetic field to power wireless sensors. Since the receiving coil is invisible and is inevitably displaced during the concrete pouring process, it is challenging to accurately determine the coil position. This leads to misalignment between the transmitting and receiving coils, which can significantly reduce the efficiency and output power [3]. Therefore, precise positioning of the embedded receiving coil is crucial.

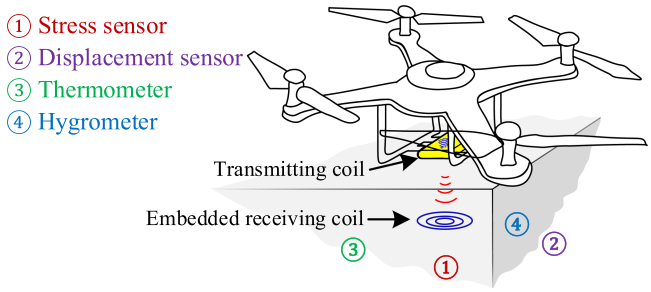

Fig. 1. Wireless sensor power supply system.

TABLE I
Comparison of Coil Positioning Methods

Methods	Positioning types	Horizontal rotation	Positioning target
[4]	2D	Effective	Transmitting coil
[5], [7]	2D	Ineffective	Transmitting coil
[6], [8]	3D	Ineffective	Transmitting coil
Proposed method	**3D**	**Effective**	**Receiving coil**

Previous researches primarily focus on positioning the transmitting coil, employing techniques based on either magnetic signal detection or voltage detection. In magnetic signal detection, the transmitting coil generates a magnetic field, which is detected by linear Hall sensors. The position of the coil is then determined using the Biot–Savart law [4]. This technique requires an additional dc source on the primary side. In voltage detection, coil positioning solutions include the lookup table method and the coupling coefficient method. In the lookup method, the positions can be obtained by matching the inductive voltages to a pre-established database [5], [6]. Nonetheless, the existing methods are ineffective when horizontal rotating occurs. In the coupling coefficient method, the coupling coefficients are calculated from the detected voltages, and the coil position is determined by analyzing the characteristics of these coupling coefficients [7], [8]. However, these methods require additional controls to switch between different operating modes. The above methods are compared in Table I. It is important to note that the

Received 17 January 2025; revised 7 March 2025 and 7 April 2025; accepted 24 April 2025. Date of publication 1 May 2025; date of current version 5 August 2025. This work was supported in part by the National Natural Science Foundation of China Joint Fund for Regional Innovation and Development under Grant U22A20222. *(Corresponding author: Yang Chen.)*

The authors are with the School of Electrical Engineering, Southwest Jiaotong University, Chengdu 611756, China (e-mail: lijingiky@my.swjtu.edu.cn; chenfuao@my.swjtu.edu.cn; zhurz@my.swjtu.edu.cn; yangchen@swjtu.edu.cn; mairk@swjtu.edu.cn).

Color versions of one or more figures in this article are available at https://doi.org/10.1109/TPEL.2025.3566391.

Digital Object Identifier 10.1109/TPEL.2025.3566391

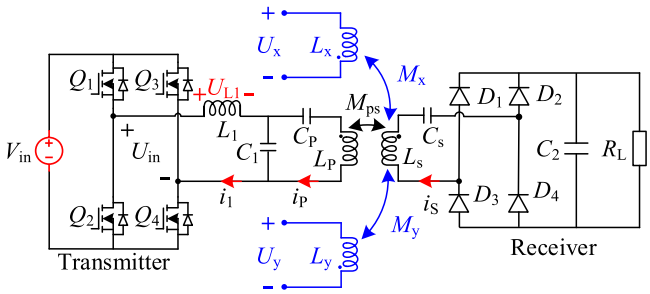

Fig. 2. Circuit topology of the proposed positioning system.

abovementioned methods are only applicable for the application where the target coil is connected to a power supply. Since the target coil of WSPS systems is embedded in cement, these methods are unsuitable in such scenarios.

This letter proposes a novel coil positioning method for WSPS systems, offering the following contributions and advantages.

1) *Decoupled transformer*: A decoupled transformer consisting of a planar coil and two solenoid coils is introduced. These coils are orthogonal and magnetically decoupled from each other.
2) *3-D receiver positioning in horizontal rotation scenarios*: The spatial coordinates of the embedded coils can be accurately determined by fitting mutual inductance surfaces and identifying intersections. Furthermore, the circular design of the receiving coil ensures consistent performance during horizontal rotation.
3) *Low-cost implementation*: The proposed method eliminates the need for additional power sources, communication modules, or complex control systems, thereby reducing the overall system cost.

II. Circuit Topology

As shown in Fig. 2, an *LCC-S* compensation network is chosen for the main circuit of the coil positioning system. L_p and L_s are self-inductances of the transmitting and receiving coils, while L_x and L_y are self-inductances of the auxiliary coils. It is worth noting that the transmitting coil is spatially orthogonally integrated with two auxiliary coils, and the mutual inductances between them are ignored. The structure is described in detail in Section III.

According to Kirchhoff's voltage law, the system can be described as follows:

$$\begin{bmatrix} U_\mathrm{in} \\ 0 \\ 0 \end{bmatrix} = \begin{bmatrix} Z_{11} & -1/(j\omega C_1) & 0 \\ -1/(j\omega C_1) & Z_{22} & -j\omega M_\mathrm{ps} \\ 0 & -j\omega M_\mathrm{ps} & Z_{33} \end{bmatrix} \begin{bmatrix} i_1 \\ i_\mathrm{p} \\ i_\mathrm{s} \end{bmatrix} \quad (1)$$

where ω is the angular frequency, Z_{11}, Z_{22}, and Z_{33} are defined in the following:

$$\begin{cases} Z_{11} = j\omega L_1 + 1/(j\omega C_1) = 0 \\ Z_{22} = j\omega L_\mathrm{p} + 1/(j\omega C_\mathrm{p}) + 1/(j\omega C_1) = 0 \\ Z_{33} = j\omega L_\mathrm{s} + 1/(j\omega C_\mathrm{s}) + R_\mathrm{ac} = R_\mathrm{ac}. \end{cases} \quad (2)$$

The relationship between U_in and V_in, as well as R_L and R_ac, can be expressed as follows:

$$U_\mathrm{in} = \frac{2\sqrt{2}}{\pi} V_\mathrm{in}, \qquad R_\mathrm{ac} = \frac{8}{\pi^2} R_L. \quad (3)$$

The fundamental currents in each circuit can be derived from (1) as shown in the following:

$$\begin{cases} i_1 = \sqrt{2}\pi V_\mathrm{in}\omega^4 {C_1}^2 {M_\mathrm{ps}}^2/(4R_L) \\ i_\mathrm{p} = -j2\sqrt{2}V_\mathrm{in}\omega C_1/\pi \\ i_\mathrm{s} = \sqrt{2}\pi V_\mathrm{in}\omega^2 C_1 M_\mathrm{ps}/(4R_L). \end{cases} \quad (4)$$

The fundamental voltages of L_1, L_x, and L_y are given by

$$\begin{cases} U_\mathrm{L1} = j\omega L_1 i_1 \\ U_\mathrm{x} = j\omega M_\mathrm{x} i_\mathrm{s} \\ U_\mathrm{y} = j\omega M_\mathrm{y} i_\mathrm{s}. \end{cases} \quad (5)$$

According to (4), when M_ps is positive, i_1 and i_s are in phase. In this case, based on (5), the polarity relationship between the U_x and U_L1 is determined by the sign of M_x: if M_x is positive, U_x and U_L1 share the same polarity, whereas if M_x is negative, they exhibit opposite polarities. Similarly, the sign of M_y determines the polarity relationship between U_y and U_L1: when M_y is positive, U_y and U_L1 have the same polarity, but when M_y is negative, their polarities are opposite. Therefore, the sign of M_x can be determined by comparing the polarities of U_x and U_L1, while the sign of M_y can be inferred from the polarities of U_y and U_L1.

By combining (4) and (5), M_{ps}, M_x, and M_y can be solved as follows:

$$\begin{cases} M_\mathrm{ps} = \sqrt{(2\sqrt{2}U_{L1}R_L)/(\pi V_\mathrm{in}\omega^3 C_1)} \\ M_\mathrm{x} = (2\sqrt{2}R_L U_\mathrm{x})/(\pi V_\mathrm{in}\omega^3 C_1 M_\mathrm{ps}) \\ M_\mathrm{y} = (2\sqrt{2}R_L U_\mathrm{y})/(\pi V_\mathrm{in}\omega^3 C_1 M_\mathrm{ps}). \end{cases} \quad (6)$$

Equation (6) indicates that M_{ps} can be obtained by measuring U_L1. Subsequently, M_x and M_y can be determined from U_x and U_y, respectively.

III. Magnetic Coupler

The magnetic coupler is shown in Fig. 3, where the turn numbers of coils L_s, L_y, L_x, and L_p are 16, 16, 16, and 15, respectively. L_x, L_y, and L_p are spatially oriented perpendicular to each other and decoupled magnetically. As a result, the mutual inductance between them is negligible.

Fig. 4 shows the simulation results of M_{ps}, M_x, and M_y for various misalignments at a 60-mm transmission distance. As shown in Fig. 4(a), M_{ps} remains positive when the *X*- and *Y*-axes misalignment range from -100 to 100 mm. In Fig. 4(b), M_x is positive when the *X*-axis misalignment is positive, and negative when the *X*-axis misalignment is negative. Similarly, Fig. 4(c) shows that M_y is positive when the *Y*-axis misalignment is positive, and negative when the *Y*-axis misalignment is negative. Therefore, the orientation of the embedded coil can be inferred based on whether M_x and M_y are positive or negative.

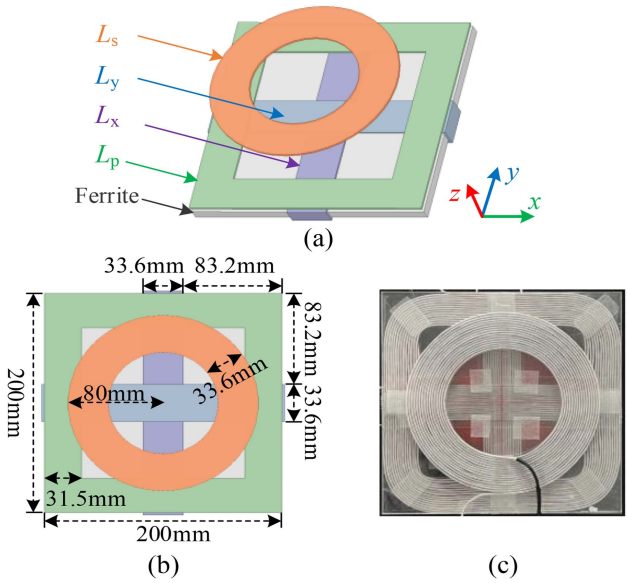

Fig. 3. Magnetic coupler (a) 3-D model, (b) top view, and (c) experimental magnetic coupler.

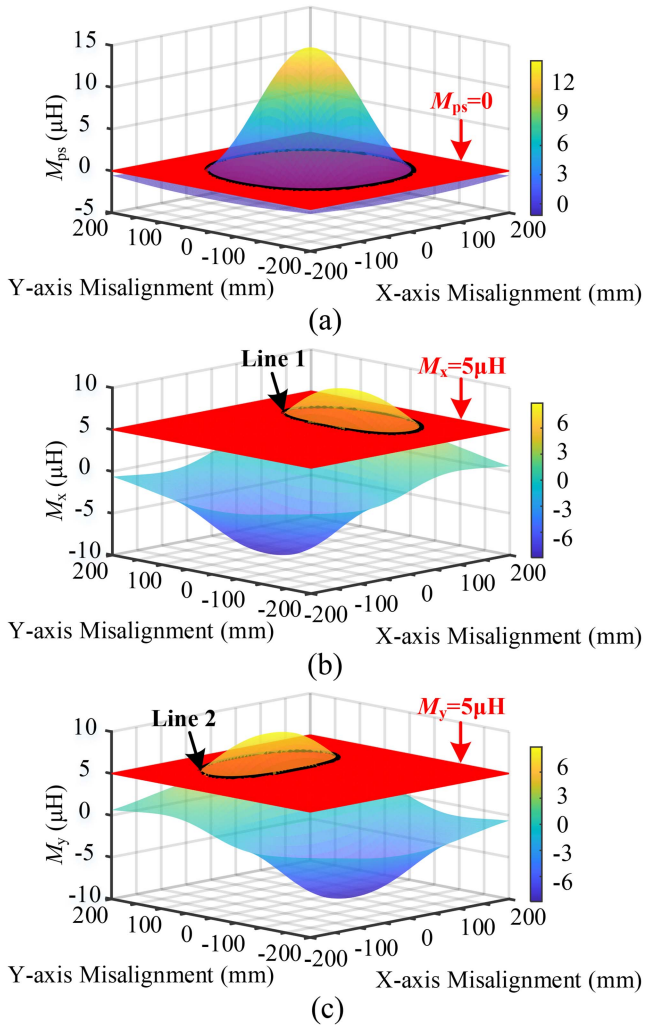

Fig. 4. (a) M_{ps}, (b) M_x, and (c) M_y for various misalignments.

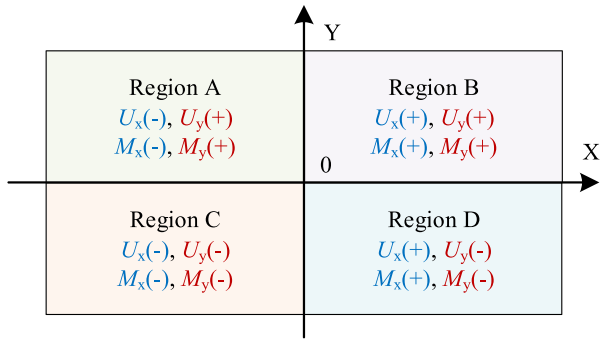

Fig. 5. Sign of voltage and mutual inductances for each region.

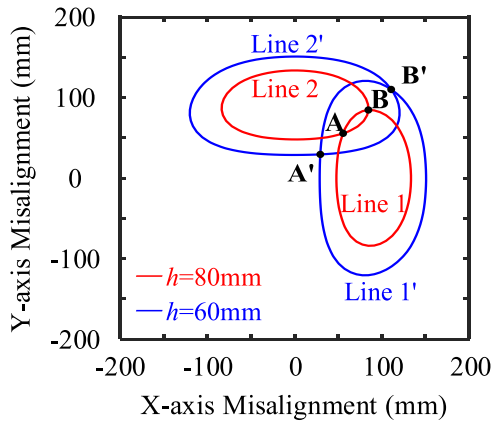

Fig. 6. Projection of the intersection lines in the XOY plane.

Assuming that the direction of U_{L1} is defined as positive, and the sign of voltages and mutual inductances for each region are illustrated in Fig. 5.

IV. Proposed Positioning Method

Mutual inductance M_{ps}, M_x, and M_y are calculated using (5). As shown in Fig. 4, two lines are derived by combining the calculation results with the simulated mutual inductance surfaces. The intersection points of these two lines indicate the possible positions of the embedded coil. When $M_x = M_y = 5\,\mu$H, the projection of the two lines in the XOY plane is shown in Fig. 6, where points A and B correspond to the possible positions of the embedded coil at an 80-mm transmission distance, points A' and B' are the possible positions at a 60-mm transmission distance.

Following the above procedure, two potential positions are identified for each transmission distance. Fig. 7 shows the spatial distribution of these possible positions. Then, the M_{ps} for these positions are obtained, and the variation of M_{ps} with X-axis misalignment is depicted in Fig. 8. As observed in Fig. 8, M_{ps} decreases monotonically as the X-axis misalignment increases. Therefore, the unique X-axis misalignment can be determined from the solution of M_{ps} in (6). Ultimately, the precise position of the embedded receiving coil can be determined. For example,

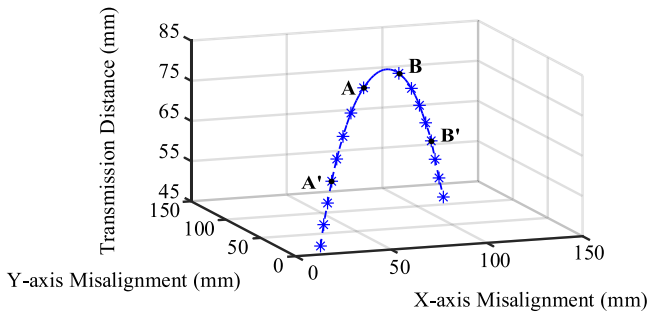

Fig. 7. Spatial distribution of possible positions.

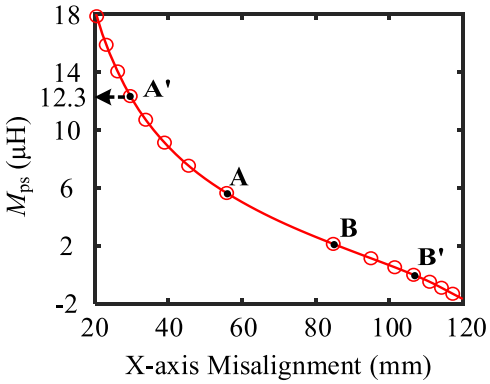

Fig. 8. M_{ps} of possible positions.

if the measured M_{ps} is 12.3 μH, the final positioning result is point A'.

In corner cases, the large misalignment may lead to relatively lower position accuracy. To align the coils precisely in these scenarios, multiple positioning and movement iterations can be performed. By iteratively adjusting equipment position until M_x and M_y fall below the predefined thresholds, precise alignment can be achieved. Once M_x and M_y are within these thresholds, the residual misalignment becomes negligible, ensuring effective alignment. Therefore, the proposed method should be integrated with a reliable movement control system to ensure effective coil alignment in practical applications. The whole process of aligning coils is shown in Fig. 9.

Fig. 10 shows the magnetic coupler before and after horizontal rotation. On one hand, since L_x, L_y, and L_p are integrated and fixed, their mutual inductance remains negligible, ensuring that (6) is valid in horizontal rotation scenarios. On the other hand, because the receiving coil is circular, the simulated mutual inductance surfaces still hold under these scenarios. Although the horizontal rotation of the transmitter changes the receiving coil's coordinates, the updated positions can be determined using the new induced voltages of the auxiliary coils. Thus, the proposed method remains effective even when horizontal rotation occurs.

V. Experimental Validation

To validate the proposed method, an experimental prototype is constructed as depicted in Fig. 11. The STM32 drives the inverter as a control element, generating 100 kHz pulsewidth modulation waveforms. Previous studies have demonstrated that concrete has little effect on the magnetic field distribution within the frequency range of hundreds of kilohertz [9], [10], [11]. To simplify the experimental setup and enhance observation, the receiving coil is placed in the air. The maximum measured mutual inductance and coupling coefficient among L_p, L_x, and

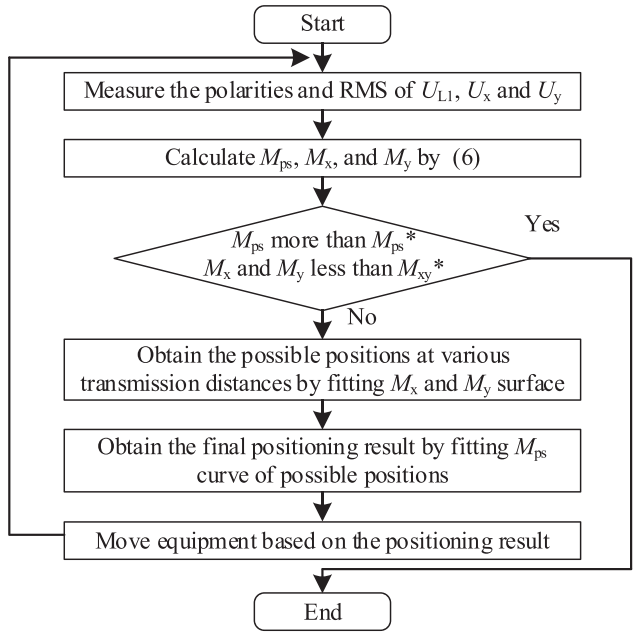

Fig. 9. Process of aligning coils.

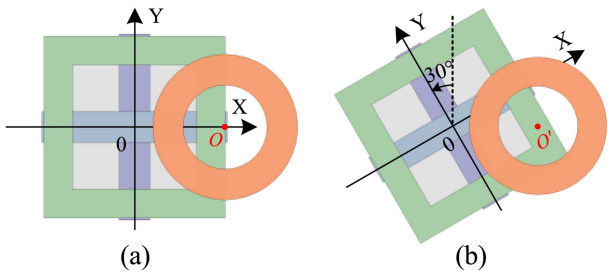

Fig. 10. Magnetic coupler. (a) Before horizontal rotation. (b) After horizontal rotation.

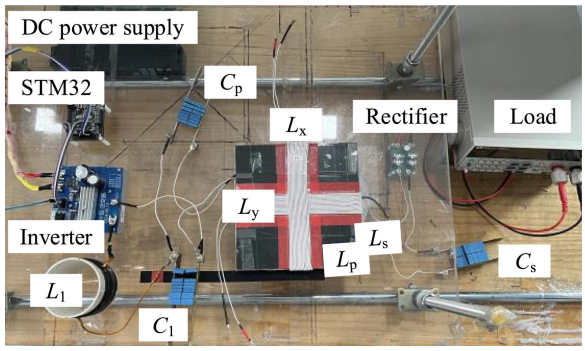

Fig. 11. Experimental prototype.

TABLE II
PARAMETERS OF EXPERIMENT PROTOTYPE

Parameter	Value	Parameter	Value
L_1	50.66 μH	C_1	50.00 nF
L_p	108.85 μH	C_p	45.90 nF
L_s	47.00 μH	C_s	43.89 nF
L_x	171.10 μH	L_y	175.14 μH
V_{in}	60 V	R_L	8 Ω

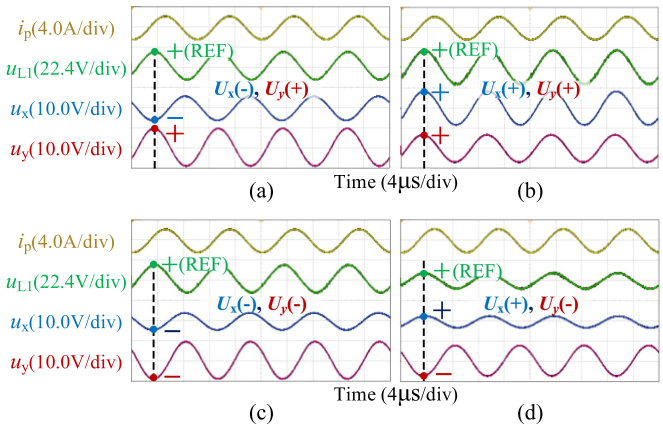

Fig. 12. Experimental waveforms of (a) (−30, 50), (b) (40, 30), (c) (−20, −50), and (d) (20, −60).

L_y are 0.86 μH and 0.0018, respectively, indicating the successful decoupling of L_p, L_x, and L_y. Other parameters of the experimental prototype are provided in Table II.

Fig. 12 shows the experimental waveform with the embedded receiving coil at (−30, 50), (40, 30), (−20, −50), and (20, −70). It can be seen that U_y and U_{L1} are in the same direction when the Y-axis misalignment is positive, whereas U_y and U_{L1} are in opposite directions when the Y-axis misalignment is negative. Meanwhile, U_x is in phase with U_{L1} when the X-axis misalignment is positive, but U_x and U_{L1} exhibit a phase difference of 180° when the X-axis misalignment is negative, which is consistent with the analysis in Section II.

Fig. 13 illustrates the positioning results at a 60-mm transmission distance. The X- and Y-axes misalignments of the actual position range from −70 to 70 mm, with increments of 20 mm. The results show that the positioning results are generally consistent with the actual positions, with 90% of the positioning accuracy within 7 mm. Positioning errors are likely attributed to measurement inaccuracies in both the actual position and voltage. These experimental results demonstrate that the proposed positioning method offers high accuracy at a 60-mm transmission distance.

Fig. 14 depicts the positioning results at various transmission distances, ranging from 50 to 80 mm in 5 mm increments. The positioning results remain largely consistent with the actual positions. Among the 64 tested locations, 93% of the positioning results fall within a 10-mm accuracy range. The errors are found to be less than 16 mm in the horizontal direction and less than 3 mm in the vertical direction. The high accuracy achieved across

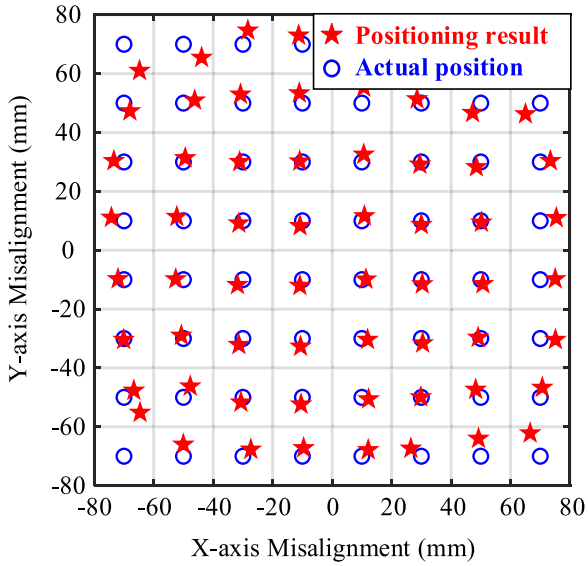

Fig. 13. Actual position and positioning result at a 60-mm transmission distance.

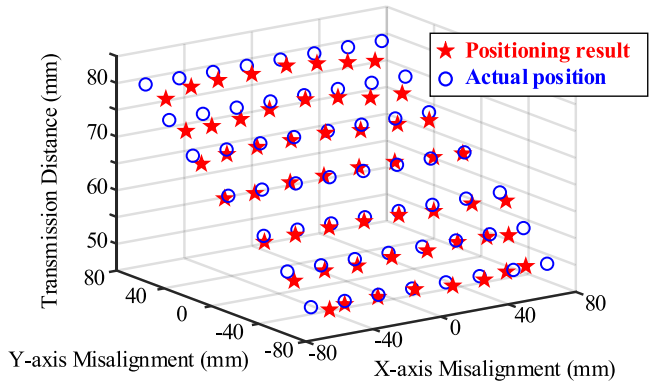

Fig. 14. Actual position and positioning result at various transmission distances.

different transmission distances further confirms the effectiveness of the proposed method.

VI. CONCLUSION

In this letter, a positioning method for receiving embedded coils based on an orthogonal decoupling transformer is proposed. By measuring the rms and phase of the voltage on the primary side, the spatial position of the receiving coil can be determined. The proposed system only requires two auxiliary coils, no communication, or any additional auxiliary. In addition, positioning and energy transfer can occur simultaneously without interference. Experimental results demonstrate that when the transmission distance is 60 mm, 90% of the position recognition accuracy falls within 7 mm in a 140 mm × 140 mm area. When the transmission distance ranges from 50 to 80 mm, 93% of the position recognition accuracy is within 10 mm. These experiments validate the effectiveness of the proposed positioning method.

REFERENCES

[1] Y. Peng, E. Ma, Q. Wang, Y. Chen, R. Mai, and U. K. Madawala, "Maximizing output power of inductive power transfer systems under rebar array shielding," *IEEE Trans. Power Electron.*, vol. 39, no. 10, pp. 13934–13945, Oct. 2024.

[2] Y. Feng, Y. Sun, T. Lin, H. Hu, and F. Chen, "Mutual inductance surrogate model of the UWPT System and its constant power optimization at misaligned positions," *Wirel. Power Transfer*, vol. 11, May 2024, Art. no. e001.

[3] Z. Chen, Z. Li, Z. Lin, J. Li, and Y. Zhang, "Mutual inductance calculation of rectangular coils at arbitrary position with bilateral finite magnetic shields in wireless power transfer systems," *IEEE Trans. Power Electron.*, vol. 39, no. 10, pp. 14065–14076, Oct. 2024.

[4] B. Zhang, Q. Chen, G. Ke, L. Xu, X. Ren, and Z. Zhang, "Coil positioning based on DC pre-excitation and magnetic sensing for wireless electric vehicle charging," *IEEE Trans. Ind. Electron.*, vol. 68, no. 5, pp. 3820–3830, May 2021.

[5] L. Tan et al., "Mesh-based accurate positioning strategy of EV wireless charging coil with detection coils," *IEEE Trans. Industr. Inform.*, vol. 17, no. 5, pp. 3176–3185, May 2021.

[6] Y. Gao, C. Duan, A. A. Oliveira, A. Ginart, K. B. Farley, and Z. T. H. Tse, "3-D coil positioning based on magnetic sensing for wireless EV charging," *IEEE Trans. Transport. Electrific.*, vol. 3, no. 3, pp. 578–588, Sep. 2017.

[7] A. Babu and B. George, "Sensor system to aid the vehicle alignment for inductive EV chargers," *IEEE Trans. Ind. Electron.*, vol. 66, no. 9, pp. 7338–7346, Sep. 2019.

[8] Z. Zhang, S. Zheng, Z. Yao, D. Xu, P. T. Krein, and H. Ma, "A coil positioning method integrated with an orthogonal decoupled transformer for inductive power transfer systems," *IEEE Trans. Power Electron.*, vol. 37, no. 8, pp. 9983–9998, Aug. 2022.

[9] S.-H. Lee, M.-Y. Kim, B.-S. Lee, and J. Lee, "Impact of rebar and concrete on power dissipation of wireless power transfer systems," *IEEE Trans. Ind. Electron.*, vol. 67, no. 1, pp. 276–287, Jan. 2020.

[10] F. Chen, N. Taylor, R. Balieu, and N. Kringos, "Dynamic application of the inductive power transfer (IPT) systems in an electrified road: Dielectric power loss due to pavement materials," *Construction. Building. Mater.*, vol. 147, pp. 9–16, Apr. 2017.

[11] Y. Peng, W. Qi, Y. Chen, R. Mai, and U. K. Madawala, "Wireless sensor power supply based on eddy currents for structural health monitoring," *IEEE Trans. Ind. Electron.*, vol. 71, no. 7, pp. 7252–7261, Jul. 2024.